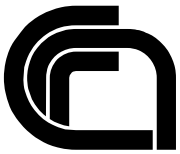

Consiglio Nazionale delle Ricerche

Understanding Vehicle-to-Vehicle IEEE 802.11p Beaconing Performance in Real-World Highway Scenarios

M. Elena Renda, G. Resta, P.Santi, F. Martelli, A. Franchini

IIT TR-16/2013

Technical report

Ottobre 2013

Istituto di Informatica e Telematica

Understanding Vehicle-to-Vehicle IEEE 802.11p Beaconing Performance in Real-World Highway Scenarios

M. Elena Renda, Giovanni Resta, Paolo Santi, Francesca Martelli, and Alessandro Franchini

IIT - CNR, Pisa – Italy

Abstract

Periodic exchange of situational information (beacons) is at the basis of most active safety applications in vehicular environments. Despite its fundamental role in raising the level of "situational awareness" onboard vehicles, very little is known to date on beaconing performance in a real vehicular environment. This paper analyzes the results of two measurement campaigns that have been designed with the purpose of disclosing beaconing performance in a variety of vehicular links, for what concerns vehicle configuration (tall/short), line-of-sight conditions (LOS/NLOS), as well as single-hop or two-hop propagation of the information reported in the beacons. For the first time, beaconing performance is characterized in terms of not only the *packet (beacon) delivery rate* (PDR), but also in terms of the *packet (beacon) inter-reception* (PIR) time. The latter metric has been suggested in the literature as more accurately measuring the level of "situation awareness" onboard vehicles than the traditional PDR metric. This paper also presents a simulation-based analysis aimed at estimating the benefit of multi-hop propagation of situational information beyond the second hop of communication. The analysis of the data collected in the measurement campaigns as well as the simulation-based analysis disclose a number of interesting insights which might prove useful in the design of active safety applications.

Finally, another major contribution of this paper is promoting the Gilbert-Elliot model, previously proposed to model bit-error bursts in packet switched networks, as a very accurate model of beacon reception behavior observed in real-world scenarios.

Index Terms

Vehicular networks, active safety applications, IEEE 802.11p, beaconing, multi-hop information propagation.

A preliminary version of this paper [17] appeared in the Proceedings of IEEE Infocom, 2012.

I. INTRODUCTION

Vehicular networks are considered a very promising technology to improve safety conditions on the road. Active safety applications are a class of applications enabled by short range vehicular radio communications aimed at raising the level of a driver's "situation awareness", with a substantial benefit in terms of improved safety conditions and better traffic efficiency. Examples of active safety applications are electronic emergency braking light, lane change assistant, lane merging assistant, intersection collision warning, etc. [26].

The successful realization of active safety applications poses hard challenges to the underlying communication technology, which should enable fast and reliable exchange of information between neighboring vehicles in an environment characterized by high mobility and typically harsh radio propagation conditions. The Dedicated Short Range Communication (DSRC) initiative [13] is aimed at defining standards at various levels of the network architecture to realize such dependable short-range radio technology for vehicular communications. In particular, the recently released IEEE 802.11p standard amends the well-known 802.11 protocol suite with the goal of improving quality in vehicular communications. The standard operates in the 5.9 GHz frequency band, and provides data rates between 3 and 27 Mbps.

The fundamental mechanism underlying active safety applications is *beaconing*, through which applications running onboard vehicles become aware of the position and status of surrounding vehicles. Beaconing consists in the periodic, single-hop broadcast transmission of status messages – called *beacons* – containing vehicle positional and kinematic data. Thus, understanding beaconing performance is a fundamental step in the process of designing active safety applications. This explains the considerable attention that the vehicular networking community has devoted to the study and optimization of beaconing [1], [5], [10], [11], [22], [24], [27]. In particular, two parameters have been identified as the most relevant to characterize beaconing performance: the *beacon delivery rate* and *beacon inter-reception time*.

Beacon delivery rate refers to the fraction of correctly received beacons over the total number of transmitted beacons in a reference time interval, i.e., it is equivalent to the well-known packet delivery rate (PDR) metric. Packet (beacon) inter-reception time (PIR) is defined as the interval of time elapsed between two successful beacon receptions, and is promoted in [5] as a metric that describes the level of "situation-awareness" achieved onboard vehicles more accurately than PDR. To understand why, consider the two following scenarios. In both scenarios, 50% of the beacons transmitted by vehicle A with a 10Hz frequency in an interval of $10\ sec$ are received at vehicle B, i.e., vehicle B receives 50 beacons in both cases. However, the reception pattern is very different. In scenario 1, beacons are received in an alternate fashion: the first beacon is received, the second is missed, the third is received, and so on. In scenario 2, beacons are received in batch: 25 beacons are received in the first 2.5 seconds of the interval, then no beacon is received for $5\ sec$, and the remaining 25 beacons are received in the last 2.5 seconds of

the interval. Clearly, scenario 1 and 2 are very different from the situation awareness viewpoint: in the former case, vehicle B's knowledge of vehicle A's position and status is outdated of at most 200 $msec$; in the latter case, there is a situation awareness blackout of at least 5 sec. Considering that a vehicle can move of more than one hundred meters in 5 sec at highway speeds, it is clear that situation awareness is severely impaired in scenario 2, resulting in possibly undetected dangerous situations. Thus, monitoring PDR values in the last, say, 10 sec can give only a rough estimate of the level of situation awareness achieved onboard, while the PIR metric is able to deliver a finer grained information.

So far, beaconing performance has been mostly studied through analysis and simulation, and only very recently a few papers evaluated beaconing PDR based on on-the-field measurements – see Section II. However, as commented above PDR alone is not sufficient to fully understand the level of situation awareness available to active safety applications. Thus, this study can be considered as the *first step towards a practical evaluation of beaconing performance* – including both PDR and PIR – based on an extensive set of *on-the-field measurements obtained in highway in presence of normal traffic conditions*. Here, normal traffic conditions refer to the fact that measurements were performed in highways regularly open to vehicular traffic, mostly during mid-morning time.

The measurement-based characterization of beaconing performance presented in this paper discloses several interesting insights:

- i) *PIR and PDR are loosely correlated metrics*, promoting PIR time as the most important metric for estimating the degree of "situation awareness" in vehicular networks. Thus, this study can be considered as an experimental validation of the observation made in [5] about the importance of the PIR metric in assessing situational awareness;
- ii) the *PIR time distribution is heavy-tailed*. More specifically, it is a power law of relatively low exponent. The *shape* of the PIR time distribution is not affected by vehicle configuration (tall/short), nor by LOS/NLOS conditions. While the shape of the PIR time distribution is not affected by vehicle configuration, the *parameters* of the distribution are profoundly impacted by vehicle configuration. As a consequence of this, important metrics such as average PIR time, occurrence of relatively long situation awareness blackouts, etc., are substantially impacted by vehicle configuration – see iv).
- iii) *relatively long situation awareness blackouts are likely to occur in batch*, also when PDR values are relatively high. This observation has important implications on active safety application design, which shall be able to cope with relatively long and repeated situation awareness blackouts;
- iv) *vehicle configuration has a moderate impact on beaconing performance*, while *LOS/NLOS conditions have a much higher impact on beaconing performance*. In particular, the probability of observing a "situation awareness" blackout of at least $1sec$ is about six times larger in NLOS than in LOS conditions;

v) *two-hop propagation* of the information reported in beacons can be used to significantly reduce the negative effect of NLOS conditions on beaconing performance. More specifically, the probability of observing a blackout event can be reduced by a factor of three with two-hops propagation, leading to a blackout probability that is only twice (instead of six times) as large as that observed in LOS conditions.

Another major contribution of this paper is presenting a methodology aimed at defining a realistic model of multihop information propagation in vehicular environments based on the collected measurement data. The obtained model is then used to simulate propagation of situational information beyond the second hop of communication. The simulation-based analysis has revealed that, while the average information propagation delay increases linearly with the number k of hops, the probability of experiencing a situation awareness blackout increases super-linearly with k, implying that propagation of situational information is effective only within 3 to 4 hops from the source vehicle. Interestingly, 3 to 4 communication hops approximately correspond to the scope of situational information relevance for active safety applications, indicating that the degraded performance of multihop information propagation for values of k larger than 4 is likely not to impact active safety application performance.

Finally, another major contribution of this paper is promoting the Gilbert-Elliot model [6], [8] as a very accurate vehicular link channel model: in the last part of the paper, it is shown that this model, which is renamed L/N model in the context of vehicular networks to emphasize effect of LineOfSight (LOS)/NonLineOfSight (NLOS) conditions on link quality, can be tuned to almost perfectly resemble the beacon reception patterns observed in our collected measurements. Given its simplicity and analytical tractability, the L/N model can be an invaluable tool in the design and analysis of active safety applications.

The rest of this paper is organized as follows. Section II discusses related work. In Section III, the hardware and software setup of the two measurement campaigns performed to evaluate beaconing performance is described. Section IV describes how the measurement campaigns were designed and performed, and how collected data has been post-processed to enable beaconing performance evaluation. The results of the first measurement campaign are presented in Section V, while Section VI discusses the results of the second measurement campaign. Section VII briefly summarizes and discusses the main results of the measurement-based study. Section VIII presents the results of a simulation-based analysis aimed at estimating the benefits of multihop propagation of situational information beyond the second hop of communication. In Section IX, the L/N model of a vehicular link is introduced, and its validity assessed by comparing the PIR time distribution generated by the model with that obtained from measurements. Finally, Section X draws the conclusions and point to some ideas to further extend the work presented in this paper.

II. Related work

Given its importance within the realm of active safety applications, beaconing performance characterization and optimization has been subject of intensive research in recent years. Most studies are based on analysis and simulation, and are typically aimed at understanding and optimizing the communication parameters (data rate, transmission power, etc.) [11], [24], [25], [27]. In [22], the authors analyze multi-hop information propagation using a simple link model, corresponding to the geometric link model that we will consider in the last part of this paper. Other studies consider specific active safety applications, such as cooperative collision warning [5], [28]. Measurement-based works are present in literature [15], [20], [23], but most of them use, as wireless network interface, different amendements of IEEE standard, like 802.11b [20], [23] or 802.11g [15].

Only very recently some papers have been published reporting results from on-the-field experiments using IEEE 802.11p compliant radios. Here, only results relevant to the beaconing application considered in this paper are discussed, while the several experimental works aimed at evaluating PHY layer features of the vehicular radio link are not considered (see, e.g., [2] and references therein).

To the best of the authors' knowledge, all existing measurement-based studies focus on PDR, and only some of them consider vehicle-to-vehicle communications.

In [10], the authors consider an intersection collision warning application, and evaluate PDR and RSSI as a function of the distance of the two vehicles from the intersection. The authors consider different transmit power values in their study, and conclude that intermediate power levels can provide good performance while at the same time reducing congestion in the wireless channel. In a similar study [16], Mangel et al. evaluates how NLOS conditions impact PDR and RSSI as vehicles approach an intersection. The effects of visibility conditions on channel quality are studied also in [9], where the authors focus on vehicle-to-infrastructure communications.

In [1], the authors present an extensive analysis of PDR in different scenarios for what concerns propagation environment, data rate, etc. The authors also analyze temporal, spatial, and symmetric correlation of PDR values, and conclude that, while temporal and spatial correlation are weak, symmetric correlation is instead quite strong.

In [18], the authors evaluate the impact of obstructions on vehicular channel quality, which is measured in terms of PDR and RSSI. Building on [18], the authors of [2] propose a radio channel model for wireless simulation accounting for vehicle obstructions.

To the best of the authors' knowledge, none of the existing measurement-based studies addresses the problem of characterizing the PIR time distribution, and its relationship with PDR and other environmental factors such as speed and distance between vehicles. As exemplified in the previous section, beacon delivery rate alone is not sufficient to quantify the level of situation awareness delivered to the active safety application. More information about the temporal pattern of successful beacon receptions is needed for this purpose, which motivated the authors

of [5] to introduce the notion of packet inter-reception time. Furthermore, none of the existing experimental work is aimed at estimating beaconing performance in different scenarios for what concerns LOS/NLOS conditions and vehicle configuration. Finally, mulithop beaconing has not been implemented nor tested on-the-field so far.

III. Experiment setup

A. Hardware configuration

Experiments have been performed using IEEE 802.11p compliant devices, namely the LinkBird-MX v3 units produced by NEC. The LinkBird-MX units are embedded Linux machines (kernel 2.6.19) based on a 64 bits MIPS processor working at 266MHz. The characteristics of LinkBird-MX 802.11p network interface are reported in Table I. LinkBird-MX units were connected to a small-size, omni-directional, $108\ mm$ long WiMo antenna with $5dBi$ gain. The antennas were mounted on the roof of the vehicles in central position as recommended in [12], [16]. The onboard equipment on each vehicle is composed of a LinkBird-MX unit, a GPS receiver, a laptop, and a rooftop antenna. In accordance with European ETSI standard, the control channel – channel 180 at 5.9 GHz – has been used for all measurements.

Parameter	Details
Frequency/Channel	$5725 - 5925$ MHz
Bandwidth	$10 - 20$ MHz
Version	IEEE802.11p Draft 3.0, July 2007
Transmit Power	Max 21 dBm (Europe)
Bitrates (10MHz)	$3, 4.5, 6, 9, 12, 18, 24, 27$ Mbps
Bitrates (20MHz)	$6, 9, 12, 18, 24, 36, 48, 54$ Mbps

TABLE I
CHARACTERISTICS OF LINKBIRD-MX 802.11P NETWORK INTERFACE.

B. The beaconing application

A beaconing application has been developed to perform the experiments. The application sends packets – henceforth called *beacons* – at a regular interval of $100ms$, according to recommendations for active safety applications [13].

Beacons are generated by the application running on the laptop, sent to the LinkBird-MX unit through an Ethernet link, and then transmitted on air using the single-hop broadcast primitive provided by the LinkBird-MX protocol stack. A packet sent in single-hop broadcast is received by all the nodes within the transmitter's communication range. Since beacons are broadcast, no packet retransmission is set.

A beacon contains the following information: the vehicle ID, the packet ID (increased by one at each transmission), the vehicle latitude, longitude, speed, heading, and current time (all taken from GPS receiver). Beacons are transmitted at full power (21 dBm in Europe) using the lowest coding rate (1/2) with BPSK modulation,

corresponding to a PHY layer raw data rate of $6Mbps$ with $20MHz$ channel bandwidth. Usage of the lowest available data rates is mandatory for active safety applications, due to the typical usage of single-hop broadcast packets (which can be sent only at the lowest data rate), and to the better communication reliability provided by the lowest data rate [7], [11].

Multi-hop propagation of situational information has also been implemented, as described in the following. Since in a real-world scenario the identity and number of vehicles encountered by a certain vehicle A in, say, the last few seconds changes significantly with time, a *dynamic* data structure should be used by the beaconing application running onboard A to store situational information of surrounding vehicles. For this purpose, the `HashMap` data structure available in Java has been used. This data structure stores `<key,value>` pairs, where `key` is the $vehicleID$, and `value` is a record reporting the situational information of the corresponding vehicle. More specifically, the `value` field reports: $packetID$, $latitude$, $longitude$, $speed$, $heading$, and $GPStime$. The $packetID$ field is used to maintain only up-to-date information in the hash table (see below).

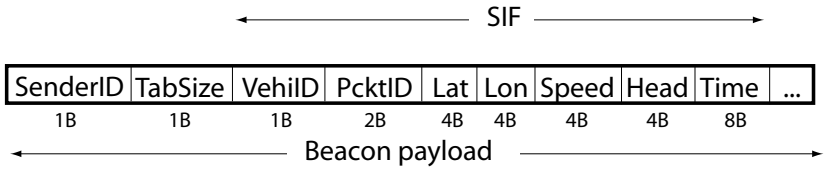

Fig. 1. Beacon format.

The beaconing application is composed of a `send` and a `receive` thread. The `send` thread prepares a new beacon and transmits the beacon every $100ms$. Before preparing the beacon, the `send` thread updates the own information in its own `HashMap` – which contains also the situational information of the sender vehicle –, increasing the $packetID$ value and updating situational information by reading data from GPS. After that, the beacon packet is prepared by introducing a *situational information field* (SIF) for each vehicle in the table – see Figure 1. The beacon payload contains also the ID of the transmitting vehicle ($senderID$), and the number of SIFs reported in the message ($TabSize$). Considering that each SIF is composed of 27 $Bytes$, and that 2 $Bytes$ are needed for the $senderID$ and $TabSize$ fields, the size of beacon payload in the experiments was 83 $Bytes$ – padded to 100 $Bytes$ to comply with recommendations about beacon size [13]. Notice that in the considered scenario it was possible to include complete situational information about the three vehicles in the beacons without exceeding the recommended beacon size. The situation is expected to be different in dense traffic scenarios, where additional techniques shall be used to keep beacon size within acceptable values, such as compression or reporting only partial situational information in the beacon. Implementation and performance estimation of techniques for multihop beaconing in presence of dense traffic conditions is beyond the scope of this paper and is left for future work.

The `receive` thread running on vehicle A, upon reception of a beacon sent by vehicle B, checks for each

vehicle whether the situational information contained in the beacon is more up-to-date than the one stored in the own `HashMap` table, and if this is the case it updates the corresponding field in the table.

Notice that since both the `send` and `receive` threads can concurrently access the `HashMap` data structure, the `Semaphore` Java class has been used to ensure mutual exclusion. Finally, the `send` and `receive` threads also produce the measurement logs, by recording in a text file each send and receive event.

IV. The measurement campaigns

Two measurement campaigns have been performed to estimate beaconing performance in a highway scenario, with different conditions for what concerns vehicle configuration, presence/absence of LOS, etc. In this section, the goals and setup of the two campaigns are described, while results are discussed in the next sections.

A. Performance metrics

Beaconing performance was evaluated according to the following metrics:

- **Packet (beacon) Delivery Rate – PDR**, defined as the ratio between the number of successfully received beacons and the total number of transmitted beacons;
- **Packet (beacon) Inter-arrival Time – PIR**, defined as the time elapsing between the reception of two successive beacons at a specific vehicle; and
- **PIR blackout**, defined as the number and distribution of blackout events, where a blackout is defined as a time interval of length $\geq 1sec$ during which no beacon is received at a specific vehicle.

The length of the time interval used to define a blackout event was empirically set to $1\ sec$, roughly corresponding to the driver's reaction time. The choice of $1\ sec$ as the reference time interval for defining blackouts is also motivated by the observation that a situational-awareness blackout of 1 or more seconds is potentially very dangerous in highway scenarios, where vehicles typically move at a speed of $30\ m/sec$ or higher.

The performance metrics defined above were directly estimated from the recorded measurement logs. The following, additional performance metric is instead *estimated* based on the recorded measurements:

- **blackout frequency**, defined as the average frequency at which blackout events occur. This metric can be estimated from the average PIR time $E(PIR)$ and the PIR blackout probability $P(BO)$ as follows:

$$BO_{freq} = \frac{P(BO)}{E(PIR)}\ . \tag{1}$$

  Equation (1) is obtained considering blackout events as independent Bernoulli trials, with success probability $P(BO)$, and observing that, on average, PIR events occur every $E(PIR)$ seconds.

The blackout frequency can be considered as an estimate of the actual blackout frequency, due to the fact that, as the results of the first measurement campaign have shown, blackout events are time correlated. Disregarding time

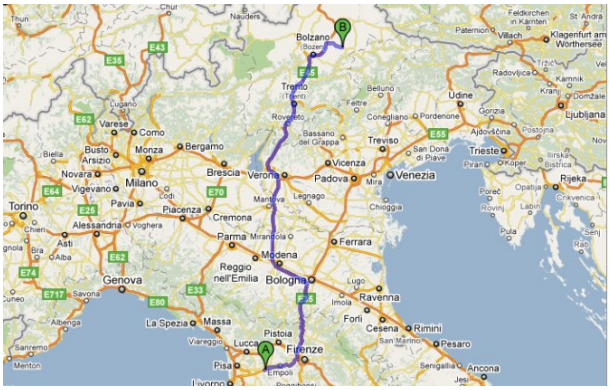

Fig. 2. Map reporting the two-way trip from Montopoli Valdarno to S.Cristina Valgardena (906 Km).

correlation in equation (1) leads to a slight under-estimation of the actual blackout frequency, quantified in about 7% in a related measurement campaign whose results are not reported here due to lack of space [14].

B. Goals

The goal of the two campaigns was to gain an in-depth understanding of beaconing performance in different conditions. Specific goals of the first measurement campaign were to:

- characterize the PIR time distribution;
- investigate the time correlation of blackout events;
- investigate correlation of PIR time vs. PDR, distance between vehicles, and speed.

Specific goals of the second measurement campaign were to:

- investigate the effect of LOS/NLOS conditions on PIR time;
- investigate the effect of short/tall vehicle configuration on PIR time;
- investigate the effect of two-hop beaconing on PIR time.

C. Trips and vehicle configuration

In the first measurement campaign, data were collected using two vehicles during a two-way trip from Montopoli Valdarno to S. Cristina Valgardena, Italy (see Figure 2) – about $900km$ two-way, and during two two-way trips from Pisa to Florence – see Figure 3 – where each two-way trip is about $176km$. Overall, measurements in this campaign were taken along a total of $1260km$ per vehicle, comprised of about $1151km$ of highways, to which the analysis reported in the following refer.

In the second measurement campaign, data were collected using three vehicles during three two-way trips from Pisa to Florence (see Figure 3). Collectively, the measurements collected in this campaign refer to about $500\ Km$ of highway driving per single vehicle.

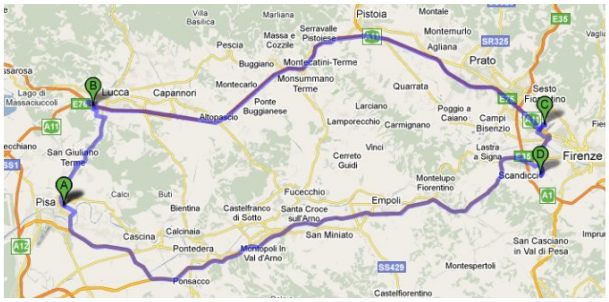

Fig. 3. Map reporting the two-way trip from Pisa to Florence (176 Km).

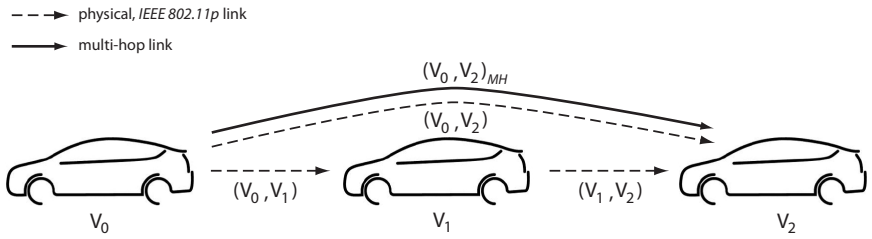

Fig. 4. Reference vehicle configuration for the second measurement campaign.

The reference vehicle configuration used in the second measurement campaign is reported in Figure 4: three vehicles are driven in a typical car-following configuration. Vehicles are named V_0 (head vehicle), V_1 (intermediate vehicle), and V_2 (tail vehicle). Three possible *physical*, IEEE 802.11p links have been considered in these measurements: the (directed) links (V_0, V_1), (V_1, V_2), and (V_0, V_2). For the pair of vehicles V_0, V_2, also the *multi-hop* link $(V_0, V_2)_{MH}$ induced by two-hop information propagation in the beaconing process has been considered, where subscript MH stands for *multi-hop*. The difference between link (V_0, V_2) and $(V_0, V_2)_{MH}$ is that the performance on the former link is measured considering only beacons received at V_2 whose sender vehicle is V_0, while the performance on the latter link is measured considering all beacons received at V_2, including those sent by V_1.

Notice that, although it was not possible to have full control of the vehicle configuration due to the fact that the measurements were conducted in real traffic conditions, the driving goal during the second measurement campaign was to have predominant LOS channel conditions for links (V_0, V_1) and (V_1, V_2), and predominant NLOS channel conditions for link (V_0, V_2). Thus, the results of this measurement campaign can be used also to carefully evaluate the impact of LOS/NLOS conditions on beaconing performance. For the reasons explained above, in the following the term *LOS links* is used to collectively refer to links (V_0, V_1) and (V_1, V_2), and the term *NLOS link* is used to refer to link (V_0, V_2).

In order to investigate the effect of different vehicle configurations on beaconing performance, and in particular the effect of tall vehicles, a different vehicle configuration was used for each of the three trips. The configurations used in the various trips are reported in Figure 5. In each configuration, there are a tall vehicle (a mini-van, height approx. $1.7m$), and two short vehicles (compact car, height approx. $1.45m$), and the position of the tall vehicle is changed across the three trips. As reported in Section VI-B, the position of the tall vehicle has a strong effect on

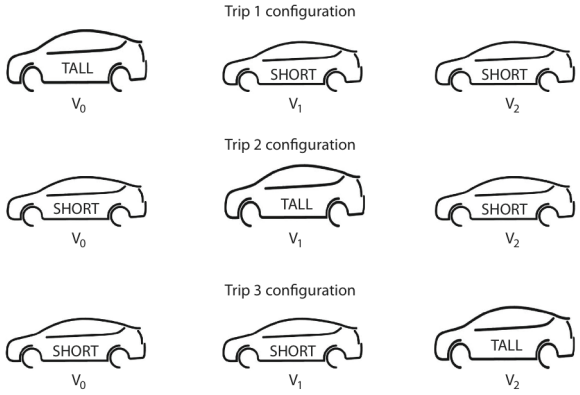

Fig. 5. Vehicle configurations in the three trips of the second measurement campaign.

the resulting beaconing performance.

D. Data post-processing

The raw traces generated during the measurement campaigns have been post-processed to generate data that can be directly used to evaluate beaconing performance.

The first addressed problem was temporal alignment of the transmit and receive traces (up to six in the experiments with three vehicles) generated for each leg of a trip. The transmit traces generated by the vehicles have been used for this purpose. Traces have been aligned using the GPS time reading. Notice that GPS devices provide time reading with a $1s$ granularity, which is insufficient for accurate temporal alignment of data traces considering that a vehicle can move of more than $30m$ in a second in a highway. However, the GPS device is polled with a 10Hz frequency (the beaconing frequency), thus allowing temporal alignment of transmit traces with an accuracy of about $0.1s$, which is sufficient for the purposes of this study (considering also the inherent inaccuracy in GPS positional data). Temporal alignment of the transmit traces allows computing the distance between vehicles during the trip.

Note that GPS position readings might be invalid for relatively long periods of time due to, e.g., galleries, reduced number of visible satellites, and so on. This implies that valid GPS readings of *all* vehicles involved in the experiments (up to three) have been recorded only for a portion of a trip. A GPS position reading taken at time t is defined to be *valid* if and only if:

a) it has been updated with respect to the previous reading taken at time $t-1$;

b) the distance between the position of the vehicle at time t and $t-1$ is compatible with the GPS speed reading, i.e.

$$d(t-1,t) \leq 1.5 \cdot v_{max} \ ,$$

where $d(t-1,t)$ is the distance between vehicle position at time t and that at time $t-1$, and v_{max} is the largest speed reading returned by GPS at times $t-1$ and t.

Criterion b) has been introduced to filter out situations in which a sudden change in environmental conditions (e.g., new satellites becoming visible) resulted in very different consecutive GPS position readings.

Once transmit traces have been temporally aligned, *valid segments* of a trip have been identified, where a valid segment is defined as a portion of a trip during which the GPS position readings of *all* vehicles are continuously valid for a time interval of at least $30s$. Intuitively, a valid segment defines a portion of a trip for which the position of all vehicles can be accurately estimated. Thus, each trip is broken down into a number of valid segments. Beaconing performance estimation reported in the remainder of this paper will be based only on the analysis of traces collected in valid segments of the various trips.

V. Results of the First Measurement Campaign

A. The PIR time distribution

What is the PIR time distribution? A first observation that can be derived from the extensive amount of collected data is that the PIR time can be considered, for all practical purposes, as a *discrete* random variable[1]. In fact, PIR values computed from the receiver traces always matched perfectly with a value of the form $k \cdot T$, where $k \geq 1$ is an integer and T is the beaconing period of $100msec$. Thus, random variable PIR denoting the time elapsing between two successive successful beacon receptions can be modeled as $PIR = k \cdot T$, where T is a constant corresponding to the beaconing period, and k is a random integer denoting the number of periods elapsed between two successful receptions.

In order to characterize PIR time distribution, it is observed that a sound notion of PIR time requires the vehicles to remain within each other transmission range during the timespan between successive successful beacon receptions. In fact, the aim of the PIR metric is to quantify the degree of situation awareness achieved *when two vehicles are within each other transmission range*. Clearly, there can be no situation awareness if two vehicles are not able to communicate.

Given the above observation, before proceeding further a notion of transmission range defined *based on the measured data* must be defined. Once the transmission range is defined, portion of the data traces during which vehicles were not continuously within each other transmission range can be filtered out and not considered in the analysis.

The transmission range can be defined by analyzing the dependence between PDR and distance between vehicles, as reported in Figure 6. It is interesting to note that there are two relatively flat regions in the PDR vs distance curve: one in the range of distances between $70m$ and $100m$, where PDR is about 30%; and one in the range of distance between $110m$ and $170m$, where the PDR is about 10%. These flat regions can be used to define

[1]This observation applies to the low channel load scenarios considered in the measurements campaign.

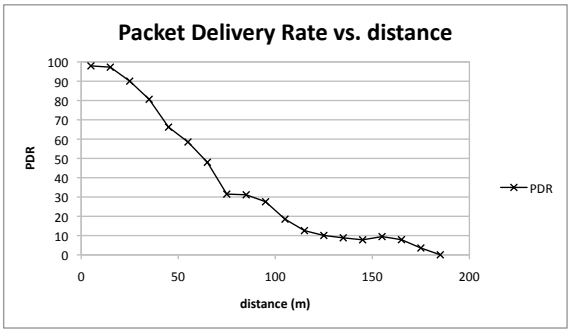

Fig. 6. PDR as a function of distance between vehicles.

a notion of transmission range, i.e., of a distance up to which beacons can be received with a given minimum reliability. More specifically, in the following two notions of transmission range are defined: a *strict* transmission range corresponding to $80m$, and a *loose* transmission range corresponding to $160m$.

It is interesting to compare the two values of transmission range resulting from the measurement campaign with those reported in the literature. In [1], the authors evaluate the PDR vs. distance function using extensive measurements in different vehicular scenarios. For all the scenarios considered, the reported transmission ranges are higher than the ones resulting from our studies. For instance, the authors of [1] report a value of PDR about 0.4 at $450\ m$. A possible reason explaining this difference in measured transmission ranges could be related to the hardware used in the experiments. In fact, while the NEC LinkBird-MX radios fullfil the requirements for minimum radio sensitivity dictated by DSRC, according to which sensitivity must be -85dBm at 3Mbs [4], in [1] the authors use radios with a much lower sensitivity of -94dBm. Thus, much longer transmission ranges can be in principle achieved using the radios of [1] given the same intensity of the received signal.

The PIR time distributions for strict and loose transmission range resulting from filtering out irrelevant portions of the data traces are reported in Figure 7. More specifically, the figure reports the complementary cumulative density function (ccdf) of random variable PIR, i.e., $P(PIR > k)$. The mean value of the PIR random variable is $126.29msec$ with strict transmission range, and $134.92msec$ with loose transmission range. The median is $100msec$ in both cases. Indeed, the PIR distribution is highly concentrated on the first term: event $(PIR = 1)$ has relative frequency 0.9344 with strict transmission range, and 0.9277 with loose transmission range. The remaining probability mass, though, is well spread among the larger terms. In fact, independently of the definition of transmission range, the PIR time ccdf is linear in log-log scale, i.e., *it is a power law*. Indeed, the following power laws almost perfectly fit experimental data:

$$P(PIR > k) = 0.065 \cdot \left(\frac{1}{k}\right)^{1.15} \quad \text{for strict tx range ,}$$

and

$$P(PIR > k) = 0.073 \cdot \left(\frac{1}{k}\right)^{1.08} \quad \text{for loose tx range ,}$$

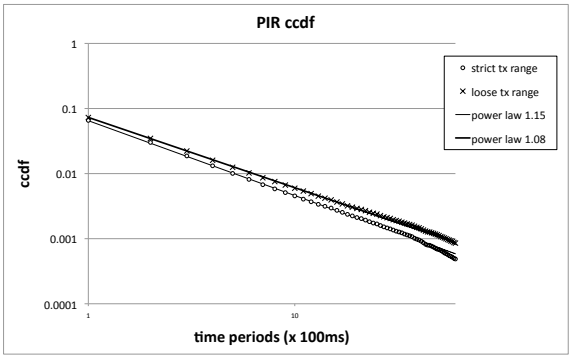

Fig. 7. PIR time ccdf and power law fitting (axes are in log scale).

What are the implications of the power law trend of PIR time? The most important implication of the power law trend is that *the PIR time distribution is heavy tailed*: the probability of having relatively long PIR time is relatively high. The above observation applies to both definitions of transmission range: not only the PIR time is a power law in both cases, but the exponent of the power law is indeed very similar.

A consequence of the observed power law trend is that, when designing active safety applications, relatively long periods of time during which situation awareness is impaired should be expected. For instance, the probability of observing a blackout event is about 0.006 with loose transmission range, which is apparently a low value. However, it should be considered that the PIR time value is sampled very frequently: on the average, a new PIR value is generated every $134.92msec$ (loose tx range). Thus, the average frequency of blackout events can be estimated as

$$BO_{freq} = 0.13492 \cdot \frac{0.006}{0.13492} \approx \frac{1}{22.5\ sec}\ .$$

Thus, a situation awareness blackout of at least $1sec$ is expected once every $22.5sec$ on average. Considering that a vehicle can easily travel for 30-40m in a highway scenario during $1sec$, it is evident that potentially dangerous situations might remain undetected during blackouts.

A third implication of the power law trend is related to modeling of the wireless link between vehicles, and will be carefully investigated in Section IX: the fact that the PIR time distribution has a fat tail is a clear evidence of the fact that the simple wireless link model often used in vehicular network analysis [22], [28], according to which a packet is successfully received within transmission range with a fixed probability $0 < p \leq 1$, does not reflect packet reception behaviors observed in real world.

B. Time-correlation of blackout events

Are blackouts isolated? The answer this question is obtained by evaluating the distribution of the first PIR event after a blackout occurs in case of loose transmission range. More formally, the evaluated quantity is the probability mass function of the conditioned event $(PIR_t = k | PIR_{t-1} > 10)$, where PIR_t is the t-th packet inter-reception time observation. The rationale for this investigation is the following: if blackouts were temporally independent

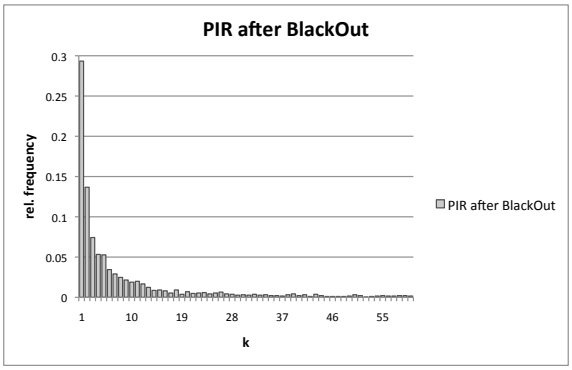

Fig. 8. Probability mass function of the PIR distribution after a blackout.

events, the shape of the PIR distribution obtained conditioning on event $PIR_{t-1} > 10$ would be very similar to the shape of the unconditioned PIR distribution. Otherwise, positive or negative temporal correlation of blackouts is displayed.

The PIR time distribution observed after a blackout is reported in Figure 8. The shape of the distribution is considerably different from that of the unconditioned PIR time distribution (see also Figure 26 later on in the paper): the probability mass of the first event is 0.2933, as compared to 0.9277 in the unconditioned distribution; the mean and median are $1.384sec$ and $250msec$, as compared to $134.9msec$ and $100msec$ in the unconditioned distribution. In general, the probability mass is shifted towards larger terms (heavier tail) in the conditioned distribution. For instance, the probability of having a blackout, which is 0.006 in the unconditioned distribution, is 0.261 after conditioning, i.e., more than 44 times larger. This clearly indicates a strong positive temporal correlation between blackout events: the fact that a blackout is just occurred considerably increases the probability of observing another blackout in the next sample. Thus, *blackout events are likely to occur in batch*, further challenging the design of effective active safety applications.

As the analysis reported in Section VI-A will clarify, blackout temporal correlation can be explained by the strong influence of LOS conditions on the vehicular link quality: if a blackout occurred, it is likely that the link between the two vehicles is in NLOS conditions; if NLOS conditions are relatively persistent, it is then very likely that also the next observed PIR time will be relatively long. This intuition is at the basis of the L/N vehicular link model which will be introduced and assessed against measured data in Section IX.

C. Correlation of PIR vs. PDR, distance, and speed

Is the PIR time distribution correlated to PDR? The answer to this question is obtained by computing the Pearson correlation coefficient[2] between PIR time measurement and the PDR observed in the 5 seconds preceding a successful reception event (which corresponds to a PIR time measurement). As seen from Table II, the coefficient

[2]The Pearson correlation coefficient takes values in $[-1, 1]$, with -1 and 1 representing maximal correlation (negative and positive, respectively), and 0 representing no correlation.

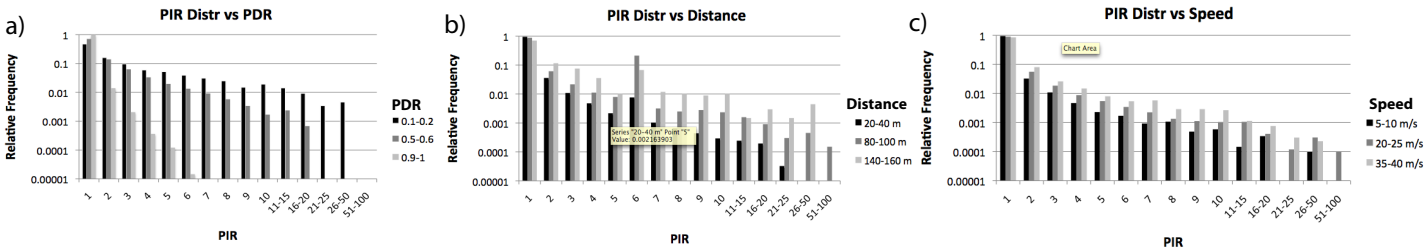

Fig. 9. PIR time distribution conditioned on PDR (left), distance (center), and speed (right). Notice the log scale in the y-axis.

reveals a weak inverse correlation between PIR and PDR. Thus, *PDR values cannot be directly used to estimate PIR time*. Since relevant PIR events from the situation awareness viewpoint are those corresponding to relatively large PIR values (say, PIR times $\geq 1sec$), correlation coefficient has also been computed on the restricted data set formed of the (PIR, PDR) pairs with $PIR \geq 10$. As seen from Table II, also in this case correlation is weak, although somewhat stronger than in case the entire data set is considered. The weak negative correlation between PIR time and PDR can be noticed also in Figure 9-a), reporting the PIR time distribution conditioned on different ranges of observed PDR values: as seen from the figure, higher PDR values tend to reduce the tail of the PIR time distribution.

PIR vs.	**All data set**	$PIR \geq 10$
PDR	-0.2313	-0.3543
distance	0.0856	0.1458
speed	0.0423	0.1084

TABLE II
CORRELATION COEFFICIENTS BETWEEN PIR TIME AND PDR, DISTANCE, AND SPEED.

Is the PIR time distribution correlated to distance? The answer to this question is obtained by computing the correlation coefficient between the PIR time and the average distance between vehicles in the time interval elapsing between consecutive successful beacon receptions. The result, reported in Table II, shows a negligible correlation between distance and PIR time, which is confirmed also by the PIR time distributions conditioned on different distance values reported in Figure 9-b). Also when restricted to PIR values ≥ 10, the correlation between distance and PIR time remains barely noticeable (see Table II).

Is the PIR time distribution correlated to speed? The answer to this question is obtained by computing the correlation coefficient between the PIR time and the average speed of vehicles in the time interval elapsing between consecutive successful beacon receptions. The result, reported in Table II, shows a negligible correlation between speed and PIR time, which is confirmed also by the PIR time distributions conditioned on different speed values reported in Figure 9-c). Also when restricted to PIR values ≥ 10, the correlation between speed and PIR time remains negligible (see Table II).

VI. Results of the Second Measurement Campaign

A. Effect of LOS/NLOS conditions

What is the effect of LOS/NLOS conditions on beaconing performance? The results reported in this section refer to the aggregate data sets collected in the three trips of the campaign. The rationale of this study is evaluating beaconing performance in what can be considered an "average" scenario, where the specific vehicle configuration (e.g, position of tall vehicles) is not known.

As can be seen from the PDR vs. distance plot reported in Figure 10, the measured transmission range in the second campaign was $150m$, hence in accordance with the *loose* transmission range measured in the first campaign. The PIR values reported in the following are then computed only considering time intervals in which the distance between vehicles V_0 and V_2 was $\leq 150m$.

The results reported in Figure 10 disclose also the noticeable effect of LOS/NLOS conditions on transmission quality: for any given value of distance, the PDR of the NLOS link (V_0, V_2) is consistently lower than the PDR of the two LOS links (V_0, V_1) and (V_1, V_2). For instance, the PDR at a distance of $100m$ is above 85% for the LOS links, while it is less than 50% for the NLOS link. At higher distances, the transmission quality drop is even more noticeable: at $150m$, the PDR for LOS links is about 60-70%, while it is about 13% (a 5-fold performance drop) for the NLOS link.

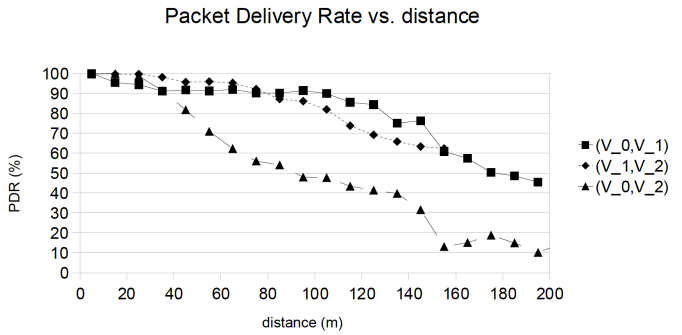

Fig. 10. PDR vs distance for the three physical links.

Considering PIR performance, a first impact of LOS/NLOS conditions is on the values of the PIR random variable: while, similarly to what observed in the first measurement campaign, the PIR values for LOS links are highly concentrated around multiples of the beaconing interval $(100ms)$, the PIR values for the NLOS link are more uniformly distributed in the time line. This is due to the fact that vehicle V_2 can receive beacons from both vehicles V_0 and V_1, and that the transmission times of the two transmitting vehicles are not synchronized.

The average PIR time for the three links is reported in Table III, along with the average PIR time obtained in the first measurement campaign. As seen from the table, PIR performance of LOS links is consistent with the measured average PIR time obtained in the first campaign. On the contrary, average PIR time for the NLOS link is considerably higher (up to 100% higher) than that observed in LOS links. The degraded PIR performance

caused by NLOS conditions is even more evident if we consider the probability of observing a blackout event. The blackout probability for the three links, as well as that measured in the first campaign, is also reported in Table III. As seen from the table, the blackout probability in LOS links is consistent with the one obtained in the first campaign, while in the NLOS link it is up to 6 times higher with respect to the LOS links, *indicating a much higher frequency of potentially dangerous situational awareness blackouts in NLOS conditions*. This comment is more tangible if we consider the average frequency of blackout events, which is one event every $26.6sec$ for link (V_0, V_1), a blackout every $18.7sec$ for link (V_1, V_2), and a blackout every $8sec$ for link (V_0, V_2). Notice that the latter situation corresponds to having a situational awareness blackout of at least $1sec$ every $8sec$, which is likely unacceptable from an active safety application point of view. As described in Section VI-C, multi-hop propagation of beaconing information can play a fundamental role to reduce the occurrence of situational awareness blackouts in NLOS links.

Link	Avg. PIR time	Blackout probability
(V_0, V_1)	$133msec$	0.005
(V_1, V_2)	$150msec$	0.008
(V_0, V_2)	$267msec$	0.033
Campaign 1	$135msec$	0.006

TABLE III
AVERAGE PIR TIME AND BLACKOUT PROBABILITY.

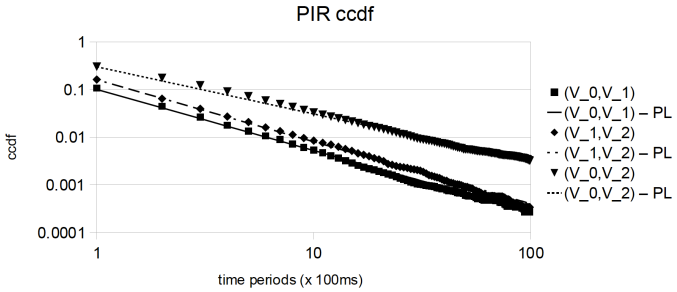

Fig. 11. PIR time ccdf for the three physical links. The figure also reports the power law fits for the three PIR time distributions.

The complementary cumulative density function (ccdf) of the PIR time distribution for the three links is reported in Figure 11. The linear trends in the log-log scale clearly indicate a power law behavior of the PIR time ccdf for the three links, which is in accordance with what observed in the first measurement campaign. The parameters of the three power laws reported in Figure 11 are reported in Table IV. As seen from the table, the exponent of the power law is very different depending on LOS/NLOS conditions: it is 1.28–1.3 for LOS links, while it is much lower (0.99) for the NLOS link, indicating a much heavier tail of the PIR time distribution.

B. Effect of vehicle configuration

What is the effect of vehicle configuration on LOS link performance? Depending on the vehicle configuration, LOS links are classified as either TS (Tall ahead vehicle and Short following vehicle), ST (Short ahead vehicle

Link	k	α
(V_0, V_1)	0.1	1.28
(V_1, V_2)	0.16	1.3
(V_0, V_2)	0.3	0.99
Campaign 1	0.073	1.08

TABLE IV
POWER LAW FITS OF TYPE $Prob(PIR > T) = k \cdot \left(\frac{1}{T}\right)^{\alpha}$ FOR THE PIR TIME CCDF OF THE THREE LINKS, AND POWER LAW FIT OBTAINED IN THE FIRST MEASUREMENT CAMPAIGN.

and Tall following vehicle), or SS (Short ahead vehicle and Short following vehicle). LOS links classification in the various trips is reported in Table V. As seen from the table, each of the LOS link categories occurs twice in the three trips, indicating a similar statistical significance of the results reported in the following.

Link	Trip 1	Trip 2	Trip 3
(V_0, V_1)	TS	ST	SS
(V_1, V_2)	SS	TS	ST

TABLE V
LOS LINKS CLASSIFICATION IN THE THREE TRIPS OF THE SECOND MEASUREMENT CAMPAIGN.

The PDR vs. distance for the three classes of LOS links is reported in Figure 12. As seen from the plots, *vehicle configuration has a very strong influence on PDR performance*. The presence of a tall vehicle is beneficial to PDR performance, especially if the tall vehicle is the following vehicle: for instance, at a distance of $100m$ the observed PDR is nearly 0 for SS links, it is about 75% for TS links, and it is about 90% for ST links. The better link quality in TS and ST configurations is likely due to the fact that, when transmission occurs between vehicles of different heights, the portion of the vehicle roofs in the Fresnel zone is *less* than in the case of vehicles with similar heights – see Figure 13. In fact, it is known that a more obstructed environment in the Fresnel zone tends to decrease signal quality at the receiver [19].

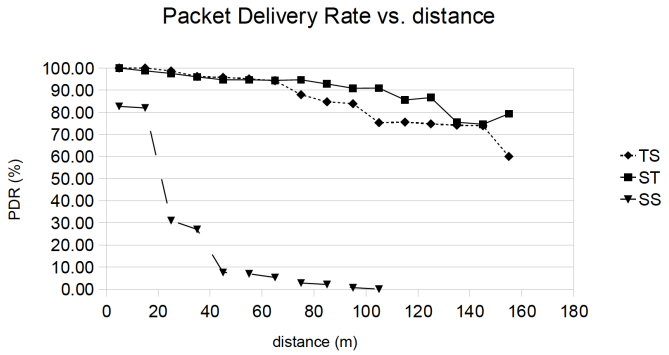

Fig. 12. PDR vs. distance for the three classes of LOS links.

The average PIR time for the three classes of links is reported in Table VI, along with the blackout probabilities. As seen from the table, *PIR performance is heavily influenced by vehicle configuration*, to a much higher extent than PDR performance. In particular, comparing ST and SS links, which display best and worst PIR performance, respectively, it can be observed that in SS links the average PIR time is increased of about 53% with respect to ST

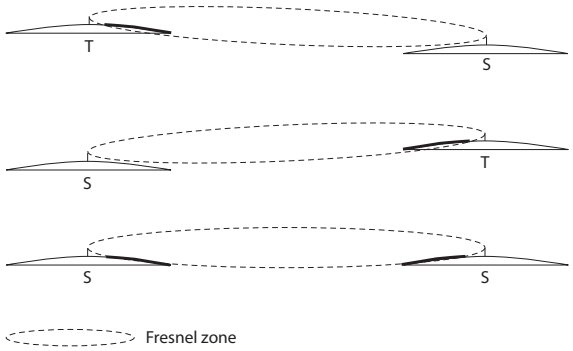

Fig. 13. Fresnel zones for TS (top), ST (middle), and SS (bottom) links. The portion of vehicle roofs in the Fresnel zone is in bold.

links, while the blackout probability is increased of over 700 times. The average frequency of blackout events is one every $2422sec$ for ST links, while it is one every $13.9sec$ for SS links. The radically different PIR performance for the SS and ST classes of links is evident also from Figure 14, which reports the PIR time ccdfs. The power law nature of the PIR time distribution is still evident, although the exponent of the power law is very different: it is 1.25 for the SS links and 3.15 for the ST links.

Link	Avg. PIR time	Blackout probability
TS	$115msec$	0.0003
ST	$109msec$	$4.5 \cdot 10^{-5}$
SS	$167msec$	0.012

TABLE VI
AVERAGE PIR TIME AND BLACKOUT PROBABILITY FOR THE THREE CLASSES OF LOS LINKS.

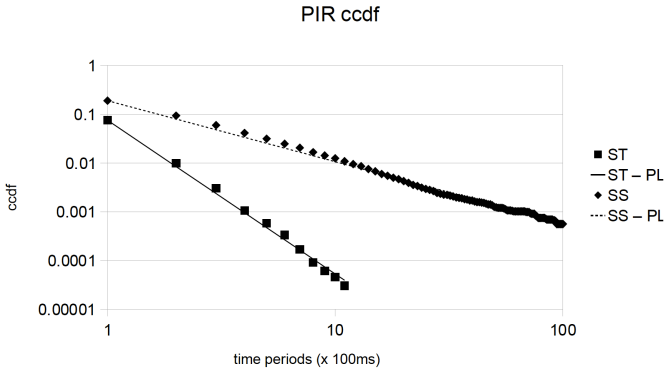

Fig. 14. PIR time ccdf for the SS and ST LOS links. The figure also reports the power law fits for the two PIR time distributions.

What is the effect of vehicle configuration on NLOS link performance? The answer to this question is obtained by analyzing performance of the NLOS link (V_0, V_2) in three different configurations which, similarly to the previous section, are called TS, ST, and SS. In TS configuration, the transmitting vehicle is tall, the receiving vehicle is short, and the in-between vehicle is short – see Figure 5. The two other configurations are defined similarly – please refer to Figure 5.

The PDR performance of the NLOS link in different configurations is reported in Figure 15. From the figure, it is evident that the ST link performs much better than both TS and SS links. Differently from the LOS link case,

performance of the TS link is only slightly superior to SS link performance.

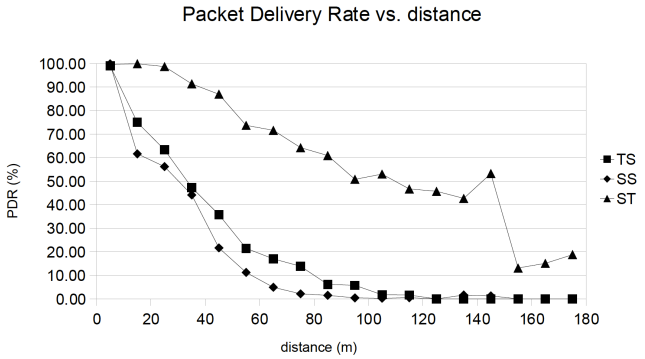

Fig. 15. PDR vs. distance for the three classes of NLOS links.

The average PIR time and the blackout probability for the three classes of NLOS links are reported in Table VII. Similarly to the case of LOS links, *PIR performance is more profoundly impacted by vehicle configuration than PDR performance*. Comparing performance of ST (best performing) vs. SS (worst performing) link, the average PIR time in the best configuration is about three times lower than in the worst configuration, and the blackout probability is about 7 times smaller. Concerning average frequency of blackout events, it is observed a blackout event every $6.6sec$ with the SS link, and a blackout event every $14.5sec$ with the ST link. Notice that in the SS configuration the in-between vehicle is tall, while in the two other configurations the in-between vehicle is short. Thus, the notable difference in performance between SS and ST configuration is likely to be due to the exacerbated NLOS conditions in SS configuration.

Link	Avg. PIR time	Blackout probability
TS	$340msec$	0.058
SS	$575msec$	0.087
ST	$173msec$	0.012

TABLE VII
AVERAGE PIR TIME AND BLACKOUT PROBABILITY FOR THE THREE CLASSES OF NLOS LINKS.

The PIR time ccdfs for the SS and ST NLOS links are reported in Figure 16. The plots clearly indicate a much heavier tail of the PIR time distribution for the SS link. It is also interesting to observe that while the PIR time distribution behaves like a power law for the SS link, the power law fit is less accurate in reproducing the behavior of the ST link.

C. Effect of two-hop information propagation

The results presented in the previous sections have highlighted that NLOS channel conditions significantly decrease beaconing performance, leading to likely unacceptable beaconing performance from an active safety application viewpoint (e.g., an average of 1 blackout event every $8sec$).

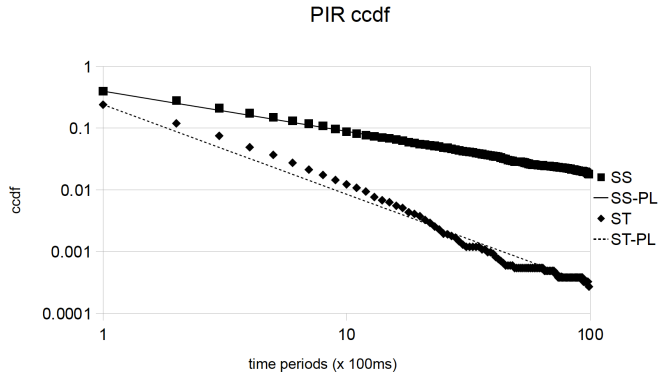

Fig. 16. PIR time ccdf for the SS and ST NLOS links. The figure also reports the power law fits for the two PIR time distributions.

Can two-hop propagation of beaconing information be used to improve performance on NLOS links? The answer to this question is obtained by comparing performance of the NLOS physical link (V_0, V_2) with that of the corresponding NLOS multihop link $(V_0, V_2)_{MH}$.

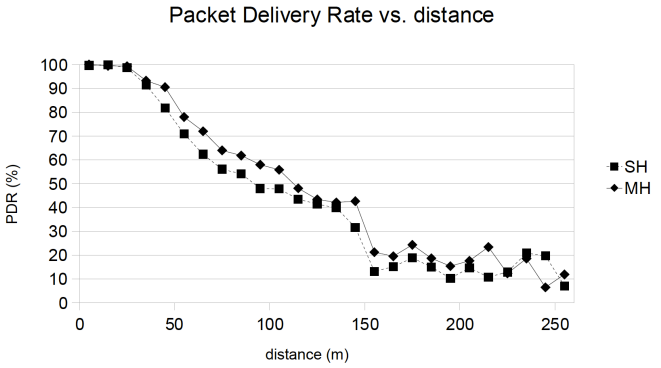

Fig. 17. PDR vs. distance for single- and multi-hop NLOS links.

Unless otherwise stated, the results reported in the following refers to the aggregate data collected in the three trips of the second measurement campaign. The PDR of the single-hop and multi-hop NLOS link is reported in Figure 17. As seen from the figure, *two-hop information propagation only modestly improves PDR performance*. The most notable performance increase can be observed in the range of distances between $50m$ and $100m$, where PDR is increased of about 7–10% with respect to the single-hop link. Differently from PDR performance, *PIR time performance is very positively affected by two-hop information propagation*. As seen from Table VIII, the average PIR time is reduced of about 43% thanks to two-hop information propagation, and the blackout probability is reduced of a factor of 3 with respect to the single-hop NLOS link. The average frequency of blackout events is reduced from 1 event every $8sec$ with the single-hop link to 1 event every $16sec$ with the multi-hop link. The fact that PIR performance with two-hop information propagation is considerably improved with respect to the single-hop case in spite of a limited PDR performance improvement should not be surprising, since the results reported in Section V-C have shown that PDR beaconing performance is only loosely correlated with PIR performance.

Figure 18 reports the PIR time ccdf of the single- and multi-hop NLOS link. The much heavier tail of the

Link	Avg. PIR time	Blackout probability
SH	$267msec$	0.033
MH	$177msec$	0.011

TABLE VIII
AVERAGE PIR TIME AND BLACKOUT PROBABILITY FOR THE SINGLE-HOP AND MULTI-HOP NLOS LINK.

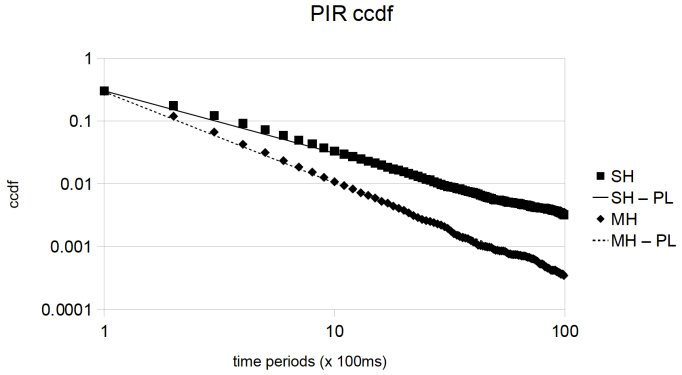

Fig. 18. PIR time ccdf for the single- and multi-hop NLOS links. The figure also reports the power law fits for the two PIR time distributions.

single-hop PIR time distribution can be clearly seen from the plots. It is also interesting to observe that the power law behavior is displayed also by the multi-hop NLOS link.

It is interesting to analyze beaconing performance in the most challenging configuration for the NLOS link, namely, the one in which the tall vehicle is in-between two short vehicles (Trip 2). This configuration is interesting since the single-hop NLOS link is in the worst configuration, while the two LOS links that are used to realize two-hop information propagation are in the best (ST) and second-best (TS) configuration – recall the results presented in Section VI-B. Thus, a very noticeable beaconing performance benefit induced by two-hop information propagation is expected with this vehicle configuration.

The analysis of the measurements collected during Trip 2 of the second campaign fully confirms the above intuition. The PDR and PIR beaconing performance in this configuration are reported in Figure 19, Table IX, and Figure 20, respectively. PDR is increased of up to 36%, and the benefit of two-hop information propagation is clearly noticeable in the range of distances 10–$150m$. The average PIR time with two-hop information propagation is reduced of about 60% with respect to the single-hop link, and the blackout probability is decreased of a factor 4. The resultant average frequency of blackout events is reduced from 1 event every $6.6sec$ in the single-hop link to 1 event every $10.5sec$ in the multi-hop link. It is interesting to observe – Figure 20 – that the multi-hop NLOS link PIR time distribution in Trip 2 can still be approximated with a power law, although the fit is less accurate than with the single-hop link.

Link	Avg. PIR time	Blackout probability
SH	$575msec$	0.087
MH	$230msec$	0.022

TABLE IX
AVERAGE PIR TIME AND BLACKOUT PROBABILITY FOR THE SINGLE-HOP AND MULTI-HOP NLOS LINK IN TRIP 2.

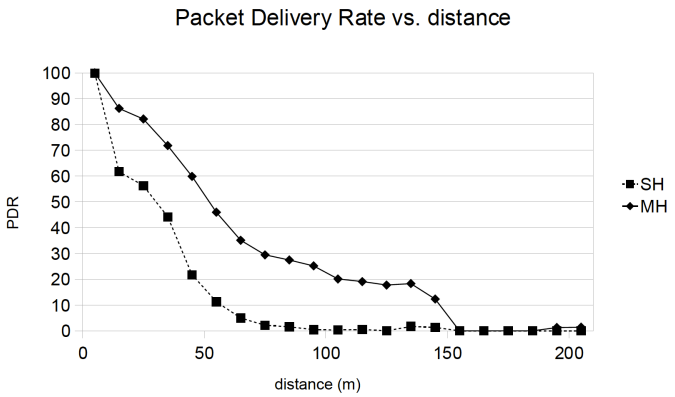

Fig. 19. PDR vs. distance for the single- and multi-hop NLOS links in Trip 2.

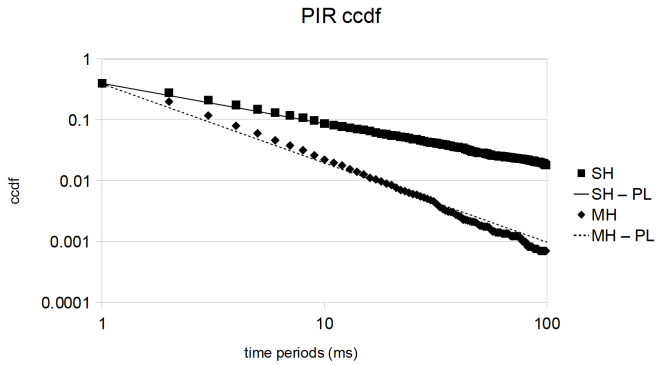

Fig. 20. PIR time ccdf for the single- and multi-hop NLOS links in Trip 2. The figure also reports the power law fits for the two PIR time distributions.

VII. Discussion

Link	Avg. PIR time	Blackout probability	Blackout frequency	PL fit (k, α)
Campaign 1	$135msec$	0.006	$1/22.5sec$	0.073, 1.08
(V_0, V_1)	$133msec$	0.005	$1/26.6sec$	0.1, 1.28
(V_1, V_2)	$150msec$	0.008	$1/18.7sec$	0.16, 1.3
(V_0, V_2)	$267msec$	0.033	$1/8sec$	0.3, 0.99
LOS–TS	$115msec$	0.0003	$1/383sec$	0.18, 1.2
LOS–ST	$109msec$	$4.5 \cdot 10^{-5}$	$1/2422sec$	0.075, 3.15
LOS–SS	$167msec$	0.012	$1/13.9sec$	0.19, 1.25
NLOS–TS	$340msec$	0.058	$1/5.86sec$	0.46, 1.1
NLOS–ST	$173msec$	0.012	$1/14.5sec$	0.24, 1.45
NLOS–SS	$575msec$	0.087	$1/6.6sec$	0.4, 0.65
NLOS–SH	$267msec$	0.033	$1/8sec$	0.3, 0.99
NLOS–MH	$177msec$	0.011	$1/16sec$	0.29, 1.45
NLOS–SS–SH	$575msec$	0.087	$1/6.6sec$	0.4, 0.65
NLOS–SS–MH	$230msec$	0.022	$1/10.4sec$	0.39, 1.3

TABLE X
PIR time characteristics of the different vehicular links considered in our study.

Table X summarizes the PIR time performance of the various vehicular links considered in this study. Some considerations are in order to comprehensively discuss the results of the experiments.

Concerning vehicular link behavior, it is interesting to observe that the measured PIR time distributions can be well approximated by a power law. In particular, power law models well the behavior of vehicular link measurements

obtained aggregating data across different vehicle configurations and LOS/NLOS conditions. In some specific NLOS links (NLOS-TS, NLOS-ST, and NLOS-SS-MH), the PIR time distribution is no longer linear in log-log scale, displaying an increasingly more pronounced decay of the PIR time ccdf for larger time values. Nevertheless, power law can still be used to satisfactorily approximate the PIR time ccdf.

It is also interesting to compare the results of this study with those obtained in the existing literature. In [18], the authors observe that the range of reliable transmission – defined as the range up to which PDR is always above 90% – was halved in presence of NLOS conditions with respect to the LOS case. Similarly to this study, the above observation refers to a scenario where NLOS conditions were due to vehicle obstructions. It is interesting to observe a similar communication range degradation in this study – see Figure 10, although in the experiments reported in this study the obstructing vehicle was much shorter than the one used in [18]. In fact, the difference in elevation between the tip of the rooftop antenna on the transmit/receive vehicles and the roof of the in-between vehicle during the second measurement campaign was only $\approx 17cm$, compared to the $36cm$ difference reported in [18]. The results reported in this study then indicate that *even a relatively modest difference in vehicle height can be sufficient to cause significant beaconing performance degradation*.

VIII. Estimation of Multhop Beaconing Beyond Second Hop

Can the benefits of multihop beaconing be estimated beyond the second hop? The data collected during the second measurement campaign has been used to estimate the benefits of multihop beaconing up to the second hop of propagation. In practical situations, the benefits of multihop propagation of situational information might extend well beyond the second hop. Since the experimental data cannot be use to estimate these benefits due to usage of only three vehicles in the measurement campaign, simulation is used to perform this analysis. More specifically, the goal of the simulation-based analysis is estimating the time needed for the situational information generated by a vehicle to reach a vehicle located k hops away, with $k = 1, \ldots, 11$.

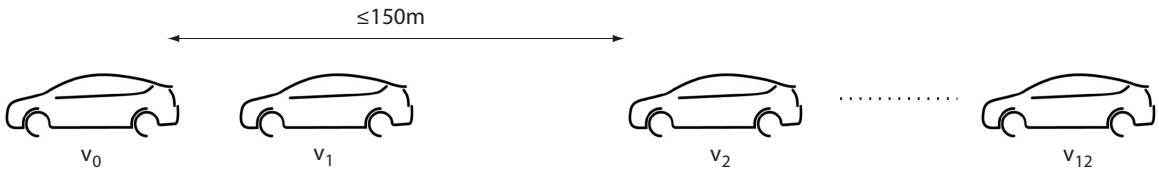

Fig. 21. Reference configuration used in the simulation experiments.

The model used to simulate propagation of situational information beyond the second hop is rooted on the findings of the experimental analyses reported in sections V and VI. A platoon composed of 12 vehicles is considered, denoted as $v_0, \ldots, v_{11}$ – see Figure 21. Inter-vehicle distances are assumed to be low enough to ensure that the distance between vehicle v_i and v_{i+2} is $\leq 150m$ for any $0 \leq i \leq 9$, to ensure that vehicles at two-hops distance are within each other transmission range – *cfr* Section VI. The specific inter-vehicle distance is not relevant as long as the

above condition is satisfied, in accordance with the observation made in Section V-C that the PIR time distribution is independent of inter-vehicle distance.

Each vehicle in the platoon sends a beacon every $100ms$, including in the beacon the more recent situational data about vehicle v_0 it is aware of. To simulate random access to a non congested channel[3], the order with which beacons are periodically sent is generated uniformly at random, and it is kept unchanged across a single simulation experiment. The beacon sent by vehicle v_i can be received only by vehicle v_{i+1} and v_{i+2}, with beacon inter-reception probabilities governed by the respective one-hop and two-hop PIR time distributions as characterized in Section VI. Due to lack of real-world data describing PIR time distribution beyond the second hop of communication, the model used in the simulations considers as zero the probability of receiving a beacon beyond the second hop. This probability, although likely very small, is not zero in a practical scenario. Hence, results reported in the following can be considered as an upper bound to the information propagation time that can be expected in practice.

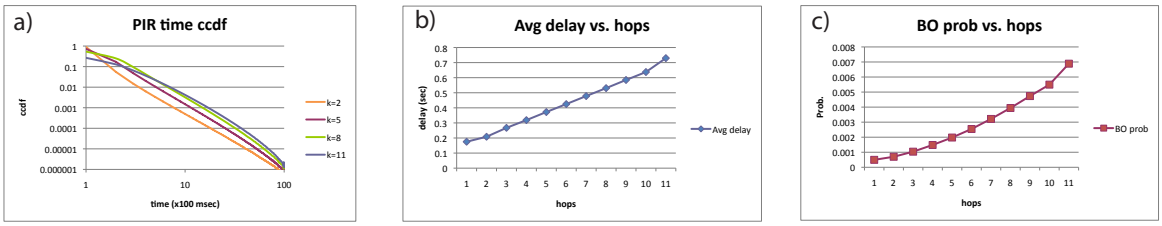

Fig. 22. Results of the simulation-based analysis: PIR time distribution (left), average delay (center), and blackout frequency (right).

The results reported in the following are the average of 10000 simulation experiments, where in a single simulation experiment each vehicle transmits 10000 beacons. Figure 22–a) reports the PIR time distributions observed at 2, 5, 8, and 11 hops from v_0. It is interesting to observe that the PIR time distribution preserves its power law shape also for number k of hops larger than two, the only difference being an increasingly heavier tail with larger values of k. It is interesting to compare the results reported in Figure 22–b) and c), reporting the average information propagation delay and the blackout probability as a function of k, respectively: while the delay displays a linear increasing trend with k, blackout probability displays a super-linear trend with k, reflecting the fact that the tail of the PIR time distribution becomes increasingly heavier with k. This indicates that the probability of experiencing a situational awareness blackout about information generated by vehicle v_0 grows quickly for large values of k. However, the relevance of this information to active safety applications running onboard vehicle v_k quickly *decreases* with k. For vehicles in the immediate surrounding of v_0 – say, up to vehicle v_4 – blackout probability only modestly increase with k, hinting to the fact that multihop propagation of situational information has the potential to substantially benefiting active safety applications.

[3]Twelve beaconing vehicles generate a data load corresponding to about 1.6% of the channel capacity.

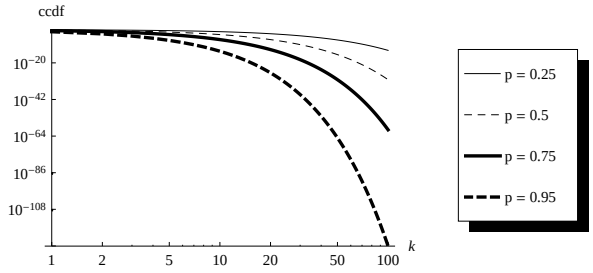

Fig. 23. Ccdf of the PIR time distribution with geometric link model and different values of parameter p.

IX. Vehicular link models

Can a simple vehicular link model resembling observed PIR time distribution be defined? The answer to this question is obtained by considering three candidate models, which are briefly introduced below. These models are aimed at modeling a situation in which the two vehicles are within each other transmission range, where the transmission range can be thought of as a value empirically defined as in Section V-A. For simplicity, and in accordance to the observation in Section V-A, in all models we assume time is discretized into $100msec$ steps and model random variable PIR as a *discrete* random variable. In the following, notation $(PIR = k)$ denotes the event "the packet inter reception time equals $k \cdot 100msec$".

A. The geometric link model

The geometric model corresponds to the well known model of independent Bernoulli trials, according to which each transmission is successfully received with a fixed probability p. Success probability p is assumed to be independent of the vehicles' speed and relative distance, as long as the two vehicles fall into each other transmission range. When the two vehicles are outside each other transmission range, the reception probability is assumed to be 0. This channel model has been used, e.g., in [22], [28].

It is straightforward to see that the geometric link model induces a PIR time distribution which is geometric of parameter p, whence the name of the model. In fact:

$$P(PIR = k) = (1-p)^{k-1}p \ ,$$

for $k = 1, 2, \ldots$.

It is also easy to see that the ccdf of the PIR time is:

$$P(PIR > k) = (1-p)^{k} \ .$$

A log-log plot of the PIR time ccdf with geometric link model and different values of p is reported in Figure 23. As seen from the plot, the tail of the PIR time distribution is very thin, unless parameter p is relatively low.

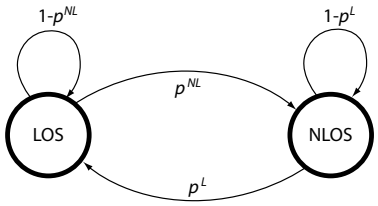

Fig. 24. The L/N link model.

B. The Gilbert model

The Gilbert model has been introduced in [8] to model bit error bursts in packet switched networks. In the Gilbert model, the link can be in two states (GOOD and BAD): when in GOOD state, the bit is correctly received with probability 1; when in BAD state, the bit is correctly received with probability $0 \leq p_{low} < 1$. Transitions between the two states are determined according to transition probabilities p_G and p_B. Thus, the model is fully characterized by three parameters: the link reception probability in BAD state p_{low}, and the two transition probabilities p_G and p_B.

The PIR time distribution in the Gilbert model can be obtained as a special case of that for the more general Gilbert-Elliot model derived in the next section. Similarly to the geometric link model, the above packet reception probabilities apply only when the two vehicles are within each other transmission range, with reception probability equal to 0 otherwise.

C. The L/N (Gilbert-Elliot) link model

In [6], Elliot introduced a generalization of the Gilbert model in which the probability of correct bit reception in GOOD state is p_{high}, with $p_{low} < p_{high} \leq 1$. The resultant model is known as the Gilbert-Elliot model. The Gilbert-Elliot model is renamed L/N model in this study, motivated by the observation made in Section VI-A that beacon reception probability is heavily influenced by LOS (corresponding to GOOD state) and NLOS (corresponding to BAD state) conditions. The resulting 2×2 Markov chain is pictorially represented in Figure 24. A link can be in either LOS or NLOS state, with transition probabilities p^L, p^{NL} determining the rate of transitions between the two states. The probability of successfully receiving a packet depends on the current link state: it is p_{high}, with $0 < p_{high} < 1$, when the link is in LOS state, and it is p_{low}, with $0 < p_{low} < p_{high}$, when the link is in NLOS state. Note that, given the memorylessness property of a Markov chain, the probability of successfully receiving a beacon at time t depends only on the state of the link at time t, and not on its state at previous time steps. Similarly to the geometric and Gilbert model, the above packet reception probabilities apply only when the two vehicles are within each other transmission range, with reception probability equal to 0 otherwise.

The Gilbert-Elliot model has been mostly used so far to characterize bit-level error burst in a communication, thus the typical quantity of interest has been the number of correctly received bits in a group of m consecutive bits. Conversely, the focus in this study is in characterizing the distribution of two consecutive successful receptions

(corresponding to packet, instead of bit, receptions), which, to the authors' best knowledge, has not been studied so far.

The first step in deriving the PIR time distribution in the L/N-model is stating a known property of the two states Markov chain defined above:

Proposition 1 (see, e.g., [3]): If $0 < p^L, p^{NL} < 1$, the unique stationary distribution of the two states Markov chain of Figure 24 is

$$\pi = \left(p_L = \frac{p^L}{p^L + p^{NL}}, \quad p_{NL} = \frac{p^{NL}}{p^L + p^{NL}} \right) \ .$$

Thus, p_L and $p_{NL} = 1 - p_L$ represent the stationary probabilities of finding the link in state LOS and NLOS, respectively.

Next, the probability $P(L|Rx)$ (respectively, $P(NL|Rx)$) of finding the link in state LOS (respectively, NLOS), conditioned on the event that a beacon has been received, is derived. Probability $P(L|Rx)$ can be computed applying Bayes' theorem:

$$\begin{aligned} P(L|Rx) &= \frac{P(Rx|L) \cdot P(L)}{P(Rx)} = \frac{p_{high} \cdot p_L}{p_L \cdot p_{high} + p_{NL} \cdot p_{low}} = \\ &= \frac{p_{high} \cdot p^L}{p^L \cdot p_{high} + p^{NL} \cdot p_{low}} \end{aligned}$$

and

$$P(NL|Rx) = 1 - P(L|Rx) = \frac{p_{low} \cdot p^{NL}}{p^L \cdot p_{high} + p^{NL} \cdot p_{low}} \ .$$

The value of $P(PIR = k)$, for any $k \geq 1$, can be computed by considering all possible unfolding of the Markov chain during k steps, starting from a reception event. Consider a given k-step unfolding of the Markov chain, i.e. a sequence of k states $S_1, \ldots, S_k$, with $S_i \in \{LOS, NLOS\}$, and let $P(S_1, \ldots, S_k)$ be the probability that the unfolding occurs. The probability that $(PIR = k)$ occurs, conditioned on unfolding $S_1, \ldots, S_k$, can be computed as follows:

$$P(PIR = k | \{S_1, \ldots, S_k\}) = p_{S_k} \cdot \prod_{i=1}^{k-1} (1 - p_{S_i}) \ ,$$

where $p_{S_i} = p_{high}$ if $S_i = LOS$, and $p_{S_i} = p_{low}$ if $S_i = NLOS$.

The probability that unfolding $S_1, \ldots, S_k$ occurs after a reception event can be computed as follows:

$$P(S_1, \ldots, S_k) = P(L|Rx) \cdot \prod_{i=1}^{k} p^{L,S_i} + P(NL|Rx) \cdot \prod_{i=1}^{k} p^{NL,S_i} \ ,$$

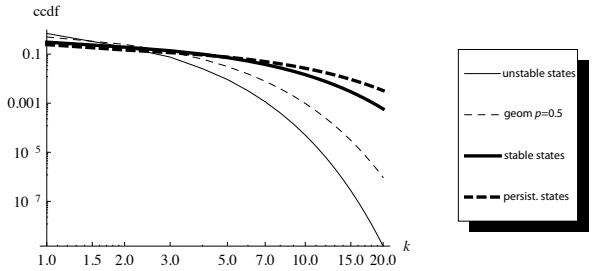

Fig. 25. Ccdf of the PIR time distribution with L/N link model and different parameter settings.

where

$$p^{L,S_1} = \begin{cases} 1 - p^{NL} & \text{if } S_1 = LOS \\ p^{NL} & \text{otherwise} \end{cases}$$

and

$$p^{L,S_i} = \begin{cases} 1 - p^{NL} & \text{if } S_{i-1} = LOS,\ S_i = LOS \\ p^{NL} & \text{if } S_{i-1} = LOS,\ S_i = NLOS \\ p^{L} & \text{if } S_{i-1} = NLOS,\ S_i = LOS \\ 1 - p^{L} & \text{if } S_{i-1} = NLOS,\ S_i = NLOS \end{cases}$$

for $i > 1$. The probabilities p^{NL,S_i} are defined similarly.

Thus, the probability of event $(PIR = k)$ can be computed as follows

$$P(PIR = k) = \sum p_{S_k} \cdot \prod_{i=1}^{k-1} (1 - p_{S_i}) \cdot P(S_1, \ldots, S_k) \ ,$$

where the summation is over all possible k-step unfolding of the Markov chain. Unfortunately, directly computing $P(PIR = k)$ requires summing a number of terms which is exponential in k, which becomes unfeasible for even moderate values of k. However, the $P(PIR = k)$ probabilities can be efficiently computed using the following recursive definition, whose correctness can be formally proved by induction (proof omitted due to lack of space):

$$P(PIR = k) = P(L|Rx)P_{kL} + P(NL|Rx)P_{kN} \ ,$$

where

$$P_{iL} = p^{NL}(1 - p_{low})P_{(i-1)N} + (1 - p^{NL})(1 - p_{high})P_{(i-1)L}$$

$$P_{iN} = (1 - p^{L})(1 - p_{low})P_{(i-1)N} + p^{L}(1 - p_{high})P_{(i-1)L}$$

for $i = 2, \ldots, k$ and

$$P_{1L} = (1 - p^{NL})p_{high} + p^{NL}p_{low}$$

$$P_{1N} = (1 - p^{L})p_{low} + p^{L}p_{high} \ .$$

The ccdf of the PIR time distribution with the L/N link model and different parameter settings is shown in Figure 25. In all the plots reported in the figure, $p_{high} = 0.9$, $p_{low} = 0.1$, and $p^L = p^{NL}$. With these settings, it is easy to see that the probability of successful reception is $p_L \cdot p_{high} + p_{NL} \cdot p_{low} = 0.5$. Different scenarios are considered, modeling a situation where transitions between LOS and NLOS states are relatively frequent ($p^L = p^{NL} = 0.8$ – *unstable* plot), relatively unfrequent ($p^L = p^{NL} = 0.2$ – *stable* plot), and seldom ($p^L = p^{NL} = 0.1$ – *persistent* plot). For comparison purposes, the plot corresponding to the geometric link model with $p = 0.5$ is also reported. As seen from Figure 25, with the L/N link model the shape of the ccdf varies considerably even if the probability of successful reception is fixed at 0.5. In particular, scenarios with relatively persistent link states result in a fatter tail of the PIR distribution.

D. Validation

Can the link models defined above be used to faithfully mimic beacon reception behavior observed in vehicular links? The answer to this question is obtained by fitting the geometric, Gilbert and L/N link models to the data obtained from first measurement campaign.

Fitting of the geometric model has been done as follows. The expected value of random variable PIR under the geometric link model is $1/p$. Thus, the parameter p of the geometric link model for a specific data set (either strict or loose transmission range) can be computed by setting $p = 1/Avg(PIR)$, where $Avg(PIR)$ corresponds to the average PIR value observed in the experiments. The resulting values of p are 0.7918 and 0.7411 in the strict and loose transmission range case, respectively.

Fitting of the Gilbert and L/N link model is less straightforward, since the models have three and four parameters, respectively, and the expected value of random variable PIR in these models cannot be readily computed. An iterative search for the best values of the model parameters is then performed, with the goal of minimizing the mean square error (in log scale).

Figure 26 reports the ccdf of the PIR time distribution derived from measurements, as well as the geometric, Gilbert and L/N model fits in case of loose transmission range. Similar results, not reported due to lack of space, have been obtained in case of strict transmission range. From the figure is seen that the geometric link model generates a packet reception behavior that deviates considerably from measured data. The Gilbert model shows a better fit to measurements than the geometric model: however, while it can be used to approximate reasonably well the tail of the distribution, it is quite inaccurate in estimating the first terms of the distribution. The L/N model can be instead be adjusted to almost perfectly fit experimental data. The resulting best fitting for the L/N model are $p^L = 0.035, p^{NL} = 0.004, p_{high} = 0.825, p_{low} = 0.0125$ in the strict transmission range case, and $p^L = 0.03, p^{NL} = 0.005, p_{high} = 0.835, p_{low} = 0.0125$ in the loose transmission range case. It is interesting to

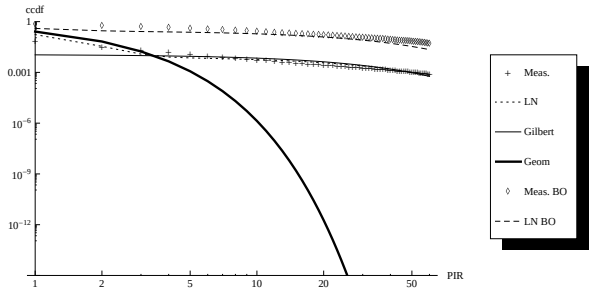

Fig. 26. Measurement-based PIR time ccdf and geometric, Gilbert, and L/N model fittings: unconditioned and conditioned distribution. (Data from the first measurement campaign.)

observe that the two best fittings of the L/N model are indeed very similar, indicating that the optimal setting of this model is not very much dependent on the choice of the transmission range.

To further validate accuracy of the L/N-model, the conditional PIR time distribution after a blackout event has been computed, as defined in Section V-A. The conditional PIR time distribution for the L/N-model has been evaluated by simulating the Markov chain with best fit parameters for 10^6 steps, and recording the observed PIR time after a blackout event. The resulting conditional PIR time distribution is reported in Figure 26, along with that obtained from measurements. As seen from the figure, the L/N-model with best fit parameters as above is able to faithfully reproduce both the unconditioned and conditioned PIR time distribution obtained from measurements. On one hand, this *validates the L/N-model as a simple, analytically tractable, and very accurate vehicular link model*. On the other hand, the fact that L/N-model can be made to almost perfectly fit measured PIR time distribution confirms the observation made from measurements that *the heavily tailed shape of the PIR time distribution is caused by transition between persistent LOS and NLOS conditions, during which reception probability is relatively high and relatively low, respectively*.

X. Conclusions

This paper reports a first extensive, measurement-based analysis of beaconing performance in vehicular networks considering not only delivery rate, but also temporal beacon reception patterns. The major findings concerning temporal correlation of successful beacon receptions is that the PIR time distribution is heavily tailed, and that situation awareness blackouts are likely to occur in batch. As discussed in the paper, these findings have important implications on the design of active safety applications, challenging the design of effective solutions.

This study also reveals the strong impact of vehicle configuration and LOS/NLOS conditions on beaconing performance. For problematic NLOS links, it is shown that a network-level solution (multi-hop information propagation) can dramatically improve beaconing performance. Scalability of the proposed solution to dense traffic scenarios is an open challenge for future work, as discussed in Section III-B.

Another major contribution of this paper is an empirical proof of the fact that the observed beacon reception patterns are caused by transition between persistent LOS and NLOS link conditions; a byproduct of this proof is the

validation of the L/N-model as a simple, analytically tractable, and very accurate vehicular link model, which can be an invaluable tool to assist active safety application designers in the challenge of developing effective solutions.

Finally, it is worth mentioning that an important avenue for future research is studying beaconing performance in presence of radio channel congestion. In fact, back-of-the-envelope calculations show that even in the largest configuration with three vehicles, the load generated by the beaconing applications[4] corresponds to only 0.4% of the available channel bandwidth. Thus, studying how beaconing performance changes in presence of increasing congestion on the radio channel is an interesting topic for future work.

REFERENCES

[1] F. Bai, D.D. Stancil, H. Krishnan, "Toward Understanding Characteristics of Dedicated Short Range Communications (DSRC) From a Perspective of Vehicular Network Engineers", *Proc. ACM Mobicom*, pp. 329–340, 2010.

[2] M Boban, T.T.V. Vinhoza, M. Ferreira, J. Barros, O.K. Tonguz, "Impact of Vehicles as Obstacles in Vehicular Ad Hoc Networks", *IEEE J. Selected Areas in Communications*, Vol. 29, n. 1, pp. 15–28, Jan. 2011.

[3] A.E.F. Clementi, C. Macci, A. Monti, F. Pasquale, R. Silvestri, "Flooding Time of Edge-Markovian Evolving Graphs", *SIAM Journal of Discrete Mathematics*, Vol. 24, n. 4, pp. 1694–1712, 2010.

[4] "Standard Specification for Telecommunications and Information Exchange Between Roadside and Vehicle Systems - 5Ghz Band Dedicated Short Range Communications (DSRC)", *ASTM E2212-03*, 2003.

[5] T. ElBatt, S.K. Goel, G. Holland, H. Krishnan, J. Parikh, "Cooperative Collision Warning Using Dedicated Short Range Wireless Communications", *Proc. ACM VANET*, pp. 1–9, 2006.

[6] E.O. Elliot, "Estimates of Error Rates for Codes on Burst-Noise Channels", *Bell Syst. Tech. J.*, Vol. 42, pp. 1977–1997, 1963.

[7] ETSI TC ITS, "Intelligent Transportation Systems (ITS): European Profile Standard on the Physical and Medium Access Layer of 5Ghz ITSs", draft ETSI ES 202 663 V.0.0.6, Oct. 2009.

[8] E.N. Gilbert, "Capacity of Burst-Noise Channel", *Bell Syst. Tech. J.*, Vol. 39, pp, 1253–1265, 1960.

[9] J. Gozalves, M. Sepulcre, R. Bauza, "IEEE 802.11p Vehicle to Infrastructure Communications in Urban Environments", *IEEE Communications Magazine*, Vol. 50, n. 5, pp. 176–183, 2012.

[10] K. Hong, D. Xing, V. Rai, J. Kenney, "Characterization of DSRC Performance as a Function of Transmit Power", *Proc. ACM VANET*, pp. 63–68, 2009.

[11] D. Jiang, Q. Chen, L. Delgrossi, "Optimal Data Rate Selection for Vehicle Safety Communications", *Proc. ACM VANET*, pp. 30–38, 2008.

[12] S. Kaul, K. Ramachandran, P. Shankar, S. Oh, M. Gruteser, I. Seskar, T. Nadeem, "Effect of Antenna Placement and Diversity on Vehicular Network Communications", *Proc. IEEE Secon*, pp. 112–121, 2007.

[13] J.B. Kenney, "Standards and Regulations", in *VANET: Vehicular Applications and Inter-Networking Technologies*, John Wiley and Sons, Chichester, UK, 2009.

[4]The load generated by the three beaconing applications equals $30 \cdot 100\ Bytes/sec = 36Kbs$.

[14] F. Librino, M.E. Renda, P. Santi, "Beaconing Perfomance in IEEE 802.11p Vehicular Networks: the Effect of Radio Channel Congestion", *Tech. Rep IIT-xx-2013*, June 2013.

[15] G. Marfia, M. Roccetti, A. Amoroso, G. Pau, "Safe driving in LA: Report from the greatest intervehicular accident detection test ever", *IEEE Trans. on Vehicular Technology*, Vol. 62, n. 2, pp. 522–535, Feb 2013.

[16] T. Mangel, M. Michl, O. Klemp, H. Hartenstein, "Real-World Measurements of Non-Line-Of-Sight Reception Quality for 5.9Ghz IEEE 802.11p at Intersections", *Proc. Nets4Cars*, pp. 189–202, 2011.

[17] F. Martelli, M.E. Renda, G. Resta, P. Santi, "A Measurement-based Study of Beaconing Performance in IEEE 802.11p Vehicular Networks, *Proc. IEEE Infocom*, pp. 1503–1511, 2012.

[18] R. Meiereles, M. Boban, P. Steenkiste, O. Tonguz, J. Barros, "Experimental Study of the Impact of Vehicular Obstructions in VANETs", *Proc. IEEE Vehicular Networking Conference (VNC)*, pp. 338–345, 2010.

[19] A.F. Molisch, *Wireless Communications*, John Wiley and Sons, Chichester, UK, 2005.

[20] M. Moske, H. Fussler, H. Hartenstein, W. Franz, "Performance measurements of a vehicular ad hoc network", *Proc. IEEE 59th VTC*, pp. 2116–2120, 2004.

[21] A. Paier, R. Tresch, A. Alonso, D. Smely, P. Meckel, Y. Zhou, N. Czink, "Average Downstream Performance of Measured IEEE 802.11p Infrastructure-to-Vehicle Links", *Proc. Workshop on Vehicular Connectivity*, 2010.

[22] G. Resta, P. Santi, J. Simon, "Analysis of Multi-Hop Emergency Message Propagation in Vehicular Ad Hoc Networks", *Proc. ACM MobiHoc*, pp. 140-149, 2007.

[23] J. Santa, M. Tsukada, T. Ernst, A. F. Gomez-Skarmeta, "Experimental analysis of multi-hop routing in vehicular ad-hoc networks", *Proc. 5th Int. Conf. TridentCom Workshops*, pp. 1–8, 2009.

[24] M. Torrent-Moreno, D. Jiang, H. Hartenstein, "Broadcast Reception Rates and Effects of Priority Access in 802.11-based Vehicular Ad Hoc Networks", *Proc. ACM VANET*, 2004.

[25] H. Venkataraman, A. d'Ussel, T. Corre, C. H. Muntean, G.-M. Muntean, "Performance analysis of real-time multimedia transmission in 802.11p based multihop hybrid vehicular networks", *Proc. 6th Int. Wireless Commun. Mobile Comput. Conf.*, pp. 1151–1155, 2010.

[26] VSC Consortium, "Vehicle Safety Communications Project Task 3 – Final Report: Indentify Intelligent Vehicle Safety Applications Enables by DSRC, *DOT HS 809 859*, March 2005.

[27] K. W. Wolterink, G. J. Heijenk, G. Karagiannis, "Information dissemination in VANETS by piggybacking on beacons - An analysis of the impact of network parameters", *Proc. IEEE Vehicular Networking Conference*, pp. 94–101, 2011.

[28] X. Yang, J. Liu, F. Zhao, N.H. Vaidya, "A Vehicle-to-Vehicle Communication Protocol for Cooperative Collision Warning", *Proc. IEEE MobiQuitous*, pp. 1–10, 2004.